2007 IEEE International Conference on
Robotics and Automation
Roma, Italy, 10-14 April 2007

Optimal Remote Center-of-Motion Location for Robotics-Assisted Minimally-Invasive Surgery

Roderick C. O. Locke and Rajni V. Patel
Canadian Surgical Technologies & Advanced Robotics (CSTAR)
339 Windermere Road, London, Ontario, N6A 5A5, Canada *and*
Department of Electrical and Computer Engineering
The University of Western Ontario
London, Ontario, N6A 5B9, Canada
rlocke@uwo.ca rajni@eng.uwo.ca

***Abstract*— A novel technique is described for isotropy-based kinematic optimization of specific robot characteristics. The new technique has advantages over existing techniques when designing robotic systems for specific, unconventional tasks, and for constrained motion. In this paper, the technique is used to assist in the selection of a remote center-of-motion (RCM) location for a research testbed that is being developed at CSTAR to study robotics-assisted minimally-invasive surgery. The optimization technique allows isotropy to be considered with respect to the surgical tool tip while operating under the RCM constraint. Global isotropy over a minimally-invasive surgical workspace is evaluated for a set of candidate RCM locations, and an optimal RCM location with respect to isotropy is selected. The isotropy results are compared with experimental data for a number of candidate RCM locations. The experimental results confirm the usefulness of the optimization technique.**

***Index Terms*— Remote center-of-motion, kinematic optimization, minimally-invasive surgery, medical robotics.**

I. Introduction

Robotics-assisted minimally-invasive surgery (RAMIS) is a surgical approach in which operations are performed using long, narrow surgical tools and an endoscope (camera), which are held by robotic arms and inserted into a patient through small incisions. Currently, there is only one FDA-approved RAMIS system available commercially – the da Vinci® system produced by Intuitive Surgical, Inc. [1]. The da Vinci has been used for many minimally-invasive procedures such as cholecystectomy (gallbladder removal) and prostatectomy (prostate removal), as well as for more challenging operations including coronary artery bypass grafting (CABG).

The work presented in this paper is part of the development at CSTAR of a research testbed for RAMIS, using two general-purpose Mitsubishi PA10-7C [2] general-purpose seven degrees-of-freedom (7-DOF) manipulators with custom-designed end-effector modules that will actuate 4-DOF endoscopic surgical tools. This paper is concerned with the problem of choosing a location for a remote center-of-motion relative to the manipulator in order to maximize performance in the RAMIS workspace. As part of this work, a novel technique for kinematic optimization was developed.

Background information is presented in Sections I-A through I-C. Section II gives an overview of the novel optimization technique. Section III describes the optimization method and results. Experimental validation of the isotropy measure is discussed in Section IV.

A. Remote Center-of-Motion

Because RAMIS is performed through small incisions in the patient's body, robotic systems for minimally-invasive surgery must pivot the surgical tools about these incisions. This pivoting constraint is called a Remote Center-of-Motion (RCM), and it is an important task for any RAMIS system, be it experimental or commercial. Several methods of generating an RCM exist. These include:

Mechanically constrained kinematic structures, such as the bar parallelogram used in the da Vinci® system [1]. In this approach, the robotic manipulator has a physical structure that pivots about the desired RCM. This approach is currently preferred for clinical RAMIS systems, since it provides high rigidity and since controller faults cannot cause the RCM constraint to be violated. Manipulators using this system are generally designed specifically for RAMIS, and cannot be used for other, more general tasks.

Passive approaches, in which the endoscopic tool is free to pivot in two degrees of freedom in order to remain aligned with the RCM. This approach was used in the Aesop® system produced by Computer Motion, Inc. (now owned by Intuitive Surgical, Inc.) [3]. This approach is considered safe, because, as with the parallel linkage approach, the RCM constraint will not be violated if a fault occurs in the controller.

Programmable or *software* constraints, in which a general-purpose robot holds the surgical tool and the control software must ensure that the tool is directed through the RCM at all times. This approach is considered less safe, since an error in the controller could lead to the RCM being violated, and as such the approach is largely restricted to research systems. However, in a non-clinical experimental setting where patient safety is not a concern, this approach to generating an RCM can be advantageous. High rigidity can be achieved using a general-purpose manipulator costing far less than a custom parallel linkage device. This approach has been used in several RAMIS research projects to date ([4], [5]).

The RAMIS testbed under development at CSTAR uses a software approach to generating the RCM. Fig. 1 depicts a PA10-7C moving about an RCM, with the base coordinate frame and "shoulder" point included for reference in later sections.

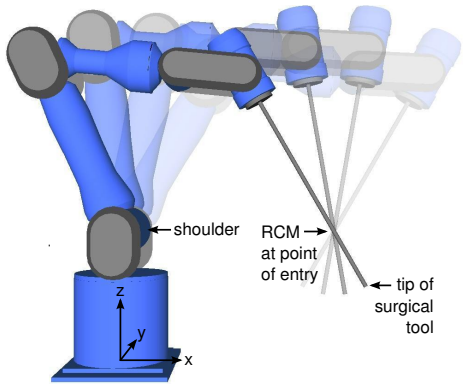

Fig. 1. Mitsubishi PA10-7C generating an RCM.

B. Kinematic Optimization

In the design of any robotic system, various parameters may be chosen. These parameters will have an impact on the eventual performance of the system. Many researchers have developed optimization metrics and algorithms to choose these parameters for improved accuracy and efficiency of motion. Salisbury and Craig [6] proposed the condition number of the Jacobian matrix as a measure of kinematic quality, while Yoshikawa [7] proposed the "manipulability measure" ($\sqrt{|\boldsymbol{J}\boldsymbol{J}^T|}$, where $\boldsymbol{J}$ is the Jacobian matrix) for the same purpose. In our system, the possible RCM locations are considered to be the design parameter.

Some research into optimization for robot design has been aimed at maximizing general kinematic quality over a broad workspace, such as Angeles' introduction of the "characteristic length" [8] to eliminate dimensional inhomogeneity in the Jacobian. Other research has focused on optimization for specific tasks. Stocco and Salcudean [9] have worked with scaling matrices in order to both resolve dimensional inhomogeneity and to take advantage of asymmetric actuation to enhance task-specific isotropy.

C. Alternative Forward Kinematics

The usual forward kinematics formulations for robotic manipulators map the joint angles to a homogeneous transformation that describes both the translation and rotation of the end-effector. However, it is possible to define other meaningful functions of the joint variables, which we call *alternative forward kinematics*.

The use of alternative forward kinematics has been explored for the purpose of control. Nakamura [10] proposed the use of a secondary "manipulation variable" to create a secondary task (for redundancy resolution), and left open the choice of kinematic functions for both the primary and secondary tasks. Seraji developed a framework called "Configuration Control" [11] that unified the use of explicit secondary tasks and objective functions – again, for the control of redundant manipulators. The "augmented" forward kinematics described in his work are equivalent to the "alternative" forward kinematics discussed here; we choose "alternative" for our terminology simply to reinforce the notion that new variables will typically *replace* one or more existing degrees of freedom, whereas in Configuration Control the new variables are usually *added* to the existing degrees of freedom for redundancy resolution.

Despite the fact that alternative forward kinematics are often used for the control of redundant manipulators, researchers studying optimization for the design of redundant manipulators do not appear to have made use of alternative forward kinematics. In most cases, such as [8], the redundancy of the manipulator is simply used to improve isotropy in the traditional six degrees of freedom. Other research, such as [9], has left the choice of kinematic functions open, but not explicitly suggested using anything other than the traditional six degrees of freedom.

To the best of our knowledge, our use of alternative forward kinematics and constraint elimination for optimization represents a novel technique. The use of alternative forward kinematics is in some ways an extension of Stocco and Salcudean's introduction of scaling matrices [9] for task-specific optimization, while the elimination of equality constraints is a common technique [12].

II. Alternative Forward Kinematics for Optimization

The use of alternative forward kinematics in optimization allows degrees of freedom that do not easily map to the traditional six (linear and angular velocity) to be directly considered. When motion is to be achieved in these new degrees of freedom, the alternative Jacobian can be used with an optimization metric. When the additional kinematic function represents a constraint, the constraint can be eliminated, and the resulting mapping can then be used.

A. Optimization for Non-traditional Motion

Consider an n-DOF manipulator that is to achieve motion in an m-DOF primary task and an $(n-m)$-DOF secondary task. Let the kinematics of the primary task be represented by the kinematic function $\boldsymbol{X}(\boldsymbol{\theta})$, and the kinematics of the secondary task by $\boldsymbol{Z}(\boldsymbol{\theta})$. Then velocities in joint space and task space are related according to:

$$\begin{bmatrix} \dot{\boldsymbol{X}} \\ \dot{\boldsymbol{Z}} \end{bmatrix} = \boldsymbol{J}_a \dot{\boldsymbol{\theta}} \tag{1}$$

where $\boldsymbol{J}_a$ is the $(n \times n)$ alternative Jacobian:

$$\boldsymbol{J}_a = \begin{bmatrix} \frac{\partial \boldsymbol{X}}{\partial \boldsymbol{\theta}} \\ \frac{\partial \boldsymbol{Z}}{\partial \boldsymbol{\theta}} \end{bmatrix} \tag{2}$$

By using the alternative Jacobian with a Jacobian-based optimization metric, the designer can ensure good motion and accuracy for both the primary and secondary tasks.

B. Optimization for Constrained Motion

By including kinematic functions for equality constraints in the alternative forward kinematics, it is possible to eliminate the constraints from the instantaneous velocity relationship. The task-space velocities can thus be related directly to those joint-space velocities that satisfy the constraints.

Consider an n-DOF manipulator with an m-DOF primary task and an $(n-m)$-DOF constraint. Let the kinematics of the primary task be represented by the kinematic function $\boldsymbol{X}(\boldsymbol{\theta})$, and those of the constraint by $\boldsymbol{Y}(\boldsymbol{\theta})$. Then joint- and task-space velocities are related by:

$$\begin{bmatrix} \dot{\boldsymbol{X}} \\ \dot{\boldsymbol{Y}} \end{bmatrix} = \boldsymbol{J}_a \dot{\boldsymbol{\theta}} \tag{3}$$

where $\boldsymbol{J}_a$ is the $(n \times n)$ alternative Jacobian:

$$\boldsymbol{J}_a = \begin{bmatrix} \frac{\partial \boldsymbol{X}}{\partial \boldsymbol{\theta}} \\ \frac{\partial \boldsymbol{Y}}{\partial \boldsymbol{\theta}} \end{bmatrix} \tag{4}$$

For the constraint kinematic function to remain at zero, $\dot{\boldsymbol{Y}} = \boldsymbol{0}$. If the alternative Jacobian does not have full rank, the optimization algorithm should assign a value corresponding to a singularity for the choice of parameter and workspace position that is being examined, and skip the rest of the analysis. If it has full rank, the Jacobian can be inverted:

$$\dot{\boldsymbol{\theta}} = \boldsymbol{J}_a^{-1} \begin{bmatrix} \dot{\boldsymbol{X}} \\ \boldsymbol{0} \end{bmatrix} \tag{5}$$

Next, the last $(n-m)$ columns of the inverted Jacobian – those that would be multiplied by $\boldsymbol{0}$ – can be eliminated. Let this new $(n \times m)$ matrix be termed the *reverse Jacobian* $\boldsymbol{J}_r$; it maps task-space velocities to joint-space velocities that maintain the current value of the constraint kinematic function:

$$\dot{\boldsymbol{\theta}} = \boldsymbol{J}_r \dot{\boldsymbol{X}} \tag{6}$$

This matrix can be used with most Jacobian-based optimization metrics – including the GII and GCI – to measure kinematic isotropy with respect to velocity while operating under an equality constraint. Note that this technique and that of Section II-A can be combined when both a non-traditional secondary task and an equality constraint are present.

III. Optimization

The Global Isotropy Index (GII) and the Culling algorithm developed by Stocco and Salcudean [9] were used in order to choose a location for the RCM of the surgical testbed. The GII provides a measure of global isotropy over the entire workspace. The Culling algorithm searches a discrete set of design parameters, and tests isotropy at positions from a discrete workspace. The GII for a given set of parameters is given by:

$$\text{GII} = \frac{\min_{\boldsymbol{X}_1 \in \text{workspace}} \sigma_{min}\left(\boldsymbol{X}_1\right)}{\max_{\boldsymbol{X}_2 \in \text{workspace}} \sigma_{max}\left(\boldsymbol{X}_2\right)} \in [0,1] \tag{7}$$

where $\sigma_{min}\left(\boldsymbol{X}_1\right)$ is the smallest singular value of the Jacobian $\boldsymbol{J}$ at workspace position $\boldsymbol{X}_1$, and $\sigma_{max}\left(\boldsymbol{X}_2\right)$ the largest singular value at position $\boldsymbol{X}_2$. A GII value of 1 indicates perfect isotropy, while a value of 0 indicates a singularity.

A. Kinematic Function for the RCM Constraint

In choosing a position for the RCM relative to the manipulator, it is desirable to achieve good isotropy of motion at the tip of the endoscopic tool while satisfying the RCM constraint. To do so, a kinematic function for the RCM constraint was derived, for use with the technique introduced in Section II-B. The kinematic function used was the RCM error – the distance between the desired RCM and the actual point of tool penetration.

A complete reference frame for the RCM may be defined, with $\hat{\boldsymbol{k}}_{\text{rcm}}$ defined to be perpendicular to the patient's skin and directed out of the body – see Fig. 2. The difference between the desired and actual penetration points in this reference frame can then be computed; let the kinematic functions $e_x(\boldsymbol{\theta})$ and $e_y(\boldsymbol{\theta})$ be defined as the x- and y-components of this difference in the reference frame of the RCM.

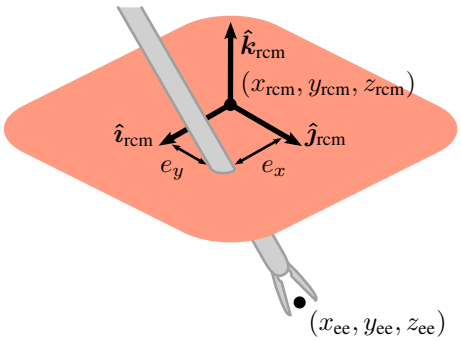

Fig. 2. RCM reference frame and alternative forward kinematics variables.

Fig. 2 depicts the RCM reference frame, surgical tool, and alternative forward kinematics variables x_{ee}, y_{ee}, z_{ee}, e_x, and e_y. The alternative forward kinematics yield the alternative Jacobian $\boldsymbol{J}_a$:

$$\boldsymbol{J}_a = \frac{\partial\left(x_{\text{ee}}, y_{\text{ee}}, z_{\text{ee}}, e_x, e_y\right)}{\partial\left(\theta_1, \theta_2, \theta_4, \theta_5, \theta_6\right)} \tag{8}$$

where θ_i is the angle of the i^{th} joint of the PA10-7C. Only five manipulator degrees-of-freedom are used; joints 3 and 7 are held at zero for the purposes of the optimization.

B. Optimization Parameters

Two design parameters were used: the x- and z-coordinates (see Fig. 1 for the base frame of reference) of the RCM, discretized into a 121×121 point grid. The y-coordinate was not varied because the PA10-7C can pivot on its first axis, rendering other candidate RCM locations equivalent to those considered. The workspace consisted of a $50\text{mm} \times 50\text{mm} \times 50\text{mm}$ cube, centered on a point 100mm directly below the RCM. This workspace is large enough for most RAMIS tasks. A 3D grid of $17 \times 17 \times 17$ discrete workspace points was chosen inside this cube.

A scaling matrix was used for the joint velocities when computing the GII, as per [9]. The diagonal terms in the matrix were set to the maximum rated speeds for the corresponding joints of the PA10-7C, as listed in [2]. This means that the computed GII values take into account the relative

speeds of the different joints – motors in the wrist of the PA10-7C are capable of far faster motion than are those in the base.

The length of the surgical tool was initially included as a design parameter in the optimization, but optimization results indicated that the shortest tool capable of reaching the entire workspace always yielded the best GII metric. The end-effector that holds and actuates the tool was therefore designed to be as short as possible while still allowing easy swapping of surgical tools; the total length of the end-effector and surgical tool is 587 mm.

C. Inverse Kinematics

While the alternative forward kinematics are theoretically sufficient for control purposes (for instance, using a Configuration Control approach), the GII optimization approach requires unique inverse kinematics solutions.

The required end-effector axis $\hat{\boldsymbol{k}}_{\text{ee}}$ can be trivially computed from the end-effector position and the RCM location:

$$\hat{\boldsymbol{k}}_{\text{ee}} = \boldsymbol{o}_{\text{ee}} - \boldsymbol{o}_{\text{rcm}} \tag{9}$$

This approach was also used in [5], and yields the homogeneous transformation that the manipulator must achieve. As mentioned in Section III-A, the third joint of manipulator was held at zero; this allowed standard closed-form inverse kinematics solutions for a 6-DOF anthropomorphic arm to be used.

D. Optimization Results

The RCM location that yielded the best GII was $(0.535, 0, -0.210)$ (meters), with a GII value of 0.0440. The GII value for every candidate RCM location was also computed for the purpose of visualization. These values are shown graphically in Fig. 3. The white background indicates RCM locations through which part or all of the workspace was unreachable, while white contours are drawn at the intervals 0.01, 0.02, 0.03, and 0.04. The RCM location having the best GII is labelled, as is the shoulder position of the PA10-7C (see Fig. 1).

E. Discussion

From Fig. 3, it is clear that isotropy is poor, with GII $\ll 1$ for all RCM locations. This is due to the long surgical tool and the RCM constraint, which together require that the PA10-7C displace its wrist over a large distance in order to achieve a small movement at the tip of the end-effector. This effect can be observed in Fig. 1, and is intrinsic to operation about an RCM. Comparable GII values have been found for the manipulators in the da Vinci® system [13]. Fig. 3 also shows that some RCM locations yield GII values that are an order of magnitude worse than the best available. These results predict that an arbitrary choice of RCM location could lead to unnecessarily large joint velocities – and an accompanying reduction in accuracy – during surgical tasks.

It was difficult to compare the standard GII approach to that using the alternative Jacobian. This was due to the lack of an obvious choice for the task scaling matrix values

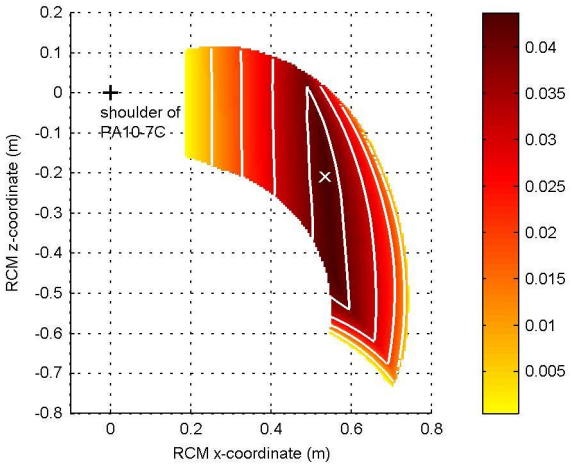

Fig. 3. GII values for candidate RCM locations. The color scale indicates the corresponding GII value for each color. Contours are drawn at intervals of 0.01, while the white 'X' indicates the optimal location.

(needed to resolve dimensional inhomogeneity [9]) in the rotational degrees of freedom. However, by choosing an arbitrary rotational task scaling coefficient of $\pi/2$ rad./s and a linear task scaling coefficient of 10 mm/s, it was possible to obtain a profile of RCM locations similar to Fig. 3 (though the GII values that resulted were much lower).

It is clear that the GII values for the standard and alternative Jacobians may correlate strongly for some choices of alternative forward kinematics. However, this correlation should not be assumed in general, as the alternative forward kinematics can introduce singularities that do not appear in the standard forward kinematics. A relevant example would be the problem of choosing an RCM location to access a *fixed* workspace. As the RCM location moves closer to the workspace, isotropy will tend to decrease due to the algorithmic singularity at the RCM [13]. The standard GII approach, in which the RCM constraint is not considered, would not detect such a singularity.

From Fig. 3, it can be seen that a range of candidate RCM locations are nearly equivalent in terms of isotropy. Because of this, additional design considerations could be used to choose between these locations, without a significant sacrifice of isotropy. In general, by using a composite optimization metric that includes the GII (or another measure of isotropy), it should be possible to combine the desire for isotropy with other design considerations.

IV. Experimental Validation

In order to allow a comparison between the GII results and the actual performance of the system, a PA10-7C manipulator was used to execute a trajectory through the workspace using a number of different RCM candidates. A helical trajectory was chosen that approached all of the edges of the workspace.

A. Control Approach

The PA10-7C was controlled using its built-in velocity-mode controller (independent joint PI control with phase compensation). Communication between a Windows PC and the robot was achieved using the ARCNET network protocol over optical fiber, with a control period of 1 ms. The PC implemented position control using the inverse kinematics approach discussed in Section III-C. Proportional control was used at the joint level, relying on the built-in velocity-mode controller of the PA10-7C to integrate the control signal.

B. Test Trajectory

For the experiment, a helical trajectory from the top to the bottom of the workspace was chosen. This trajectory approached all of the edges of the workspace – an important goal, since positions near the extremes of the workspace frequently yield the worst conditioning of the manipulator. The reference trajectory was completed in 10 seconds, with smooth acceleration and deceleration at the start and end of the trajectory. This completion time was chosen such that a small amount of error occurred even at the best-performing RCM locations, in order to provide sufficient contrast with the poorly-performing RCM locations. The average end-effector velocity over this reference trajectory was 36.4 mm/s, while the peak velocity was 54.6 mm/s.

The reference trajectory is depicted in Figs. 4 and 5, along with the actual trajectories for two different RCM locations.

C. Experimental Results

Table I shows the results for each of the 15 RCM locations that were tested. For each location, the x- and z-coordinates are given, as well as the GII value and the maximum end-effector error that was observed during the execution of the experimental trajectory. The maximum end-effector error values are plotted in Fig. 6; the color map of GII values from Fig. 3 is superimposed beneath the error data so that the relationship between the GII metric and the experimental performance can be observed. The experimental results for average end-effector error, as well as for maximum and average error at the RCM, had roughly the same relationship to one another as did the maximum end-effector error values.

TABLE I
EXPERIMENTAL RESULTS.

x_{rcm} (m)	z_{rcm} (m)	GII	Max error (mm)
0.550	-0.540	0.0357	6.3
0.630	-0.570	0.0351	6.1
0.715	-0.630	0.0148	6.1
0.530	-0.410	0.0421	5.4
0.630	-0.390	0.0340	5.3
0.720	-0.370	0.0107	5.5
0.460	-0.300	0.0356	5.3
0.535	-0.210	0.0440	5.1
0.650	-0.160	0.0139	5.2
0.350	-0.210	0.0228	6.3
0.400	-0.110	0.0293	5.4
0.430	0.010	0.0332	5.3
0.260	-0.140	0.0110	17.1
0.260	-0.060	0.0111	16.7
0.260	0.030	0.0111	16.2

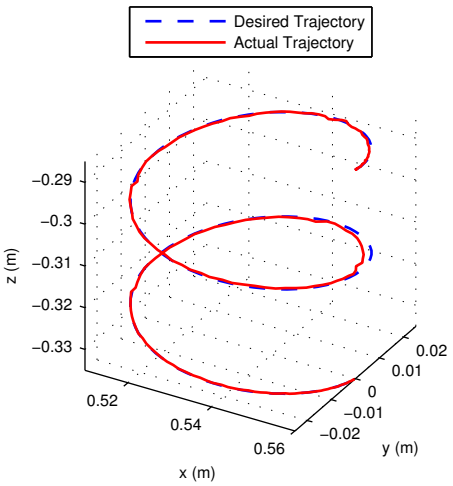

Fig. 4. Control results using RCM location $(0.535, 0, -0.210)$.

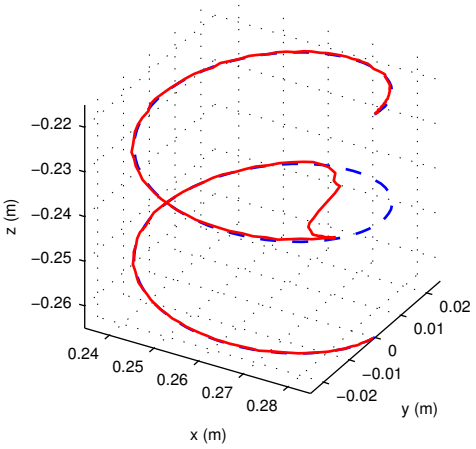

Fig. 5. Control results using RCM location $(0.260, 0, -0.140)$.

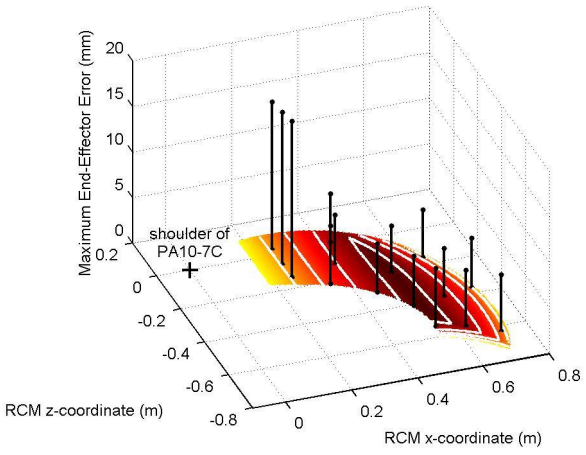

Fig. 6. Maximum end-effector error for an experimental trajectory.

Actual trajectories for two different RCM locations are depicted in Figs. 4 and 5. For the RCM location $(0.535, 0, -0.210)$ (Fig. 4), the end-effector tracked the desired trajectory well (but not perfectly), as predicted by the good GII score for this RCM location. For the RCM location $(0.260, 0, -0.140)$ (Fig. 5), which had a GII score four times worse than location $(0.535, 0, -0.210)$, significant positioning error can be observed near the halfway point in the trajectory.

D. Discussion

The RCM locations near the shoulder of the PA10-7C that have poor GII scores exhibited poor performance, as predicted. However, the RCM locations having the largest x-coordinates had better-than-expected behavior. This was mostly likely because the trajectory did not contain the locations and directions of motion through the workspace that would have proven most problematic at these RCM locations. The poor GII scores for these locations occur because the elbow of the PA10-7C becomes almost fully extended when reaching some workspace positions; movement of the end-effector in the x-direction becomes difficult near these positions. However, the trajectory required end-effector movement primarily in the y-direction near these workspace positions, and so this poor conditioning was not exposed. In contrast, for the RCM locations near the shoulder of the PA10-7C, the helical trajectory moved through the workspace positions with the poorest conditioning in the directions in which motion was most difficult, thereby exposing the poor isotropy.

Since each RCM location has its poorest performance in a slightly different workspace area and direction of motion, a very lengthy and complicated test trajectory would be needed to exercise the worst-case performance of every RCM location. This is one reason that computational approaches utilizing the conditioning of the Jacobian are preferred over simulations and experiments, since the singular value decomposition finds these "worst-case" values directly. Nevertheless, this experiment was able to show at least some correspondence between the GII metric and real-world performance.

V. Conclusions And Future Work

The GII optimization approach with alternative forward kinematics and constraint elimination successfully allowed isotropy under an RCM constraint to be evaluated, and allowed global isotropy values over a minimally-invasive surgical workspace to be compared for a number of candidate RCM locations. The effectiveness of the optimization approach was partially verified by experimental results.

We plan to investigate the use of the alternative forward kinematics developed for this optimization in a Configuration Control framework for controlling the PA10-7C. Such alternative formulations may be especially useful with a force-control approach to the generation of the RCM, since forces measured at the RCM would correspond almost directly to the alternative forward kinematics variables e_x and e_y.

We also intend to investigate ways in which the redundancy of the PA10-7C can be used to improve performance. Possible goals include the avoidance of joint limits and the maximization of isotropy. Finally, our broader project goal is to integrate the remaining system components and use the completed RAMIS testbed for research into haptics, telesurgery, and tool navigation.

Acknowledgments

This research was supported by the Ontario Research and Development Challenge Fund under grant 00-May-0709, by the Natural Sciences and Engineering Research Council (NSERC) of Canada under grant RGPIN-1345, and by infrastructure grants from the Canada Foundation for Innovation awarded to the University of Western Ontario and the London Health Sciences Centre (Canadian Surgical Technologies & Advanced Robotics).

Technical assistance for simulation and control of the PA10-7C was kindly provided by Rodrigo S. Jamisola of Colorado State University, USA, Marcelo Ang, Jr. of the National University of Singapore, and Torsten Scherer of the University of Bielefeld, Germany.

References

[1] G. S. Guthart and J. K. Salisbury, "The intuitive telesurgery system: Overview and application," in *Proc. IEEE Int. Conf. Robot. Automat.*, San Francisco, CA, USA, April 2000, pp. 618–621.

[2] *General Purpose Robot PA10 Series (PA10-7CE) Instruction Manual for Installation, Maintenance, and Safety*, Mitsubishi Heavy Industries. [Online]. Available: http://www.mhi.co.jp/kobe/mhikobe/products/mechatronic/download/new/loadfile/e_7c_m.pdf

[3] J. M. Sackier and Y. Wang, "Robotically assisted laparoscopic surgery. from concept to development," *Surgical Endoscopy*, vol. 8, pp. 63–66, 1994.

[4] M. Michelin, P. Poignet, and E. Dombre, "Dynamic task/posture decoupling for minimally invasive surgery motions," in *Proc. IEEE/RSJ Int. Conf. Intelligent Robots and Systems*, vol. 4, New Orleans, LA, USA, April–May 2004, pp. 3625–3630.

[5] H. Mayer, I. Nagy, and A. Knoll, "Kinematics and modelling of a system for robotic surgery," in *Proc. Advances in Robot Kinematics*, Sestri Levante, Italy, June 2004.

[6] J. K. Salisbury and J. T. Craig, "Articulated hands: Force control and kinematic issues," *The Int. J. Robotics Res.*, vol. 1, no. 1, pp. 4–17, 1982.

[7] T. Yoshikawa, "Manipulability of robotic mechanisms," *The Int. J. Robotics Res.*, vol. 4, no. 2, pp. 3–9, 1985.

[8] J. Angeles, F. Ranjbaran, and R. V. Patel, "On the design of the kinematic structure of seven-axes redundant manipulators for maximum conditioning," in *Proc. IEEE Int. Conf. Robot. Automat.*, Nice, France, May 1992.

[9] L. J. Stocco, S. E. Salcudean, and F. Sassani, "On the use of scaling matrices for task-specific robot design," *IEEE Trans. Robot. Automat.*, vol. 15, no. 5, pp. 958–965, October 1999.

[10] Y. Nakamura, H. Hanafusa, and T. Yoshikawa, "Task-priority based redundancy control of robot manipulators," *Int. J. Robotics Res.*, vol. 6, no. 2, pp. 3–15, 1987.

[11] H. Seraji, "Configuration control of redundant manipulators: Theory and implementation," *IEEE Trans. Robot. Automat.*, vol. 5, no. 4, pp. 472–490, August 1989.

[12] F. Cheng, T. Chen, and Y. Sun, "Resolving manipulator redundancy under inequality constraints," *IEEE Trans. Robot. Automat.*, vol. 10, no. 1, pp. 65–71, 1994.

[13] A. L. Trejos and R. V. Patel, "Port placement for endoscopic cardiac surgery based on robot dexterity optimization," in *Proc. IEEE Int. Conf. Robot. Automat.*, Barcelona, Spain, April 2005, pp. 912–917.